Available online at www.sciencedirect.com
ScienceDirect
Journal of Catalysis 244 (2006) 1–9
JOURNAL OF CATALYSIS
www.elsevier.com/locate/jcat

Surface acidity of niobium phosphate and steam reforming of dimethoxymethane over $CuZnO/Al_2O_3$–NbP complex catalysts

Qing Sun [a,b], Aline Auroux [b], Jianyi Shen [a,b,*]

[a] *Lab of Mesoscopic Chemistry, School of Chemistry and Chemical Engineering, Nanjing University, Nanjing 210093, China*
[b] *Institut de Recherches sur la Catalyse, CNRS, 2 Av. Einstein, 69626 Villeurbanne Cedex, France*

Received 14 May 2006; revised 15 July 2006; accepted 18 July 2006
Available online 25 September 2006

Abstract

Dimethoxymethane (DMM) is nontoxic and of high hydrogen content and may be used as a H_2 storage material for small H_2 sources. Steam reforming of DMM requires a bifunctional catalyst composed of an acidic component and a traditional copper catalyst, on which DMM is hydrolyzed on the acidic sites to methanol and formaldehyde, which are then further reformed to H_2 and CO_2 on metallic copper sites. In this work, samples of niobium phosphate with high surface areas were synthesized, characterized, and tested for the hydrolysis of DMM and used as acidic components for the reforming of DMM to produce H_2. The structure and surface areas of these samples were characterized, and the activity for the hydrolysis of DMM was correlated with the surface acidities. It was found that all of the niobium phosphate samples exhibited high activity for the hydrolysis of DMM. The one with a high surface area (394 m^2/g) was highly acidic with mainly Brønsted acid sites and thus was the most active for the hydrolysis of DMM among the niobium samples studied in this work. Mixing the niobium phosphate with $CuZnO/Al_2O_3$ did not affect the activity of $CuZnO/Al_2O_3$ for the reforming of methanol. The activity and selectivity to H_2 were low for the steam reforming of DMM over traditional $CuZnO/Al_2O_3$ alone. Mechanically mixing niobium phosphate with $CuZnO/Al_2O_3$ greatly enhanced the conversion of DMM (e.g., 100% at 493 K) with high selectivity to H_2. This indicates that niobium phosphate is an effective acidic component for the hydrolysis of DMM and can be used with $CuZnO/Al_2O_3$ for reforming DMM to produce H_2.

Keywords: Niobium phosphate; Hydrolysis of dimethoxymethane; Steam reforming; Hydrogen production; Adsorption microcalorimetry; Surface acidity

1. Introduction

Fuel cell systems have attracted much attention as potential electricity generation devices for household and automotive applications [1–3]. These systems have the advantages of cleanness, high energy density, compactness, and highly efficient energy transformation. Hydrogen is the most promising fuel for such applications. H_2 can be produced by steam reforming of gasoline [4], natural gas, methanol [5–8], dimethyl ether [9–11], and other products, as well as decomposition of ammonia [12–14]. However, the reforming temperatures of natural gas and gasoline are high [15] (above 873 K for natural gas and above 1073 K for gasoline), requiring significant energy input, and the stability of catalysts and refractory reactors is also problematic. Methanol is synthesized from syngas [16], and its reforming is relatively easy at around 523–573 K. The disadvantage of using methanol as an H_2 source is that it is highly toxic. Thus, reforming of dimethyl ether (DME) has been performed to produce H_2 [9–11]. However, reforming of DME might be limited by the low rate of hydrolysis.

In this work, we studied the reforming of dimethoxymethane (DMM) for the production of hydrogen. DMM is nontoxic and environmentally benign. It can be easily stored and handled, because it is a liquid under atmospheric pressure. In addition, steam reforming of DMM can be done at low temperature (below 533 K) [17]. DMM may be synthesized from direct oxidation of methanol. Liu et al. studied the oxidation of methanol to DMM using heteropoly acids [18]. Yuan et al. found that Re/γ-Fe_2O_3 was active for the oxidation of methanol to DMM [19,20]. V_2O_5/TiO_2 catalysts also have been found to be active for this reaction [17].

* Corresponding author. Fax: +86 25 83317761.
E-mail address: jyshen@nju.edu.cn (J. Shen).

0021-9517/$ – see front matter
doi:10.1016/j.jcat.2006.07.027

Steam reforming of DMM involves the hydrolysis of DMM to methanol and formaldehyde, which are further reformed to produce H_2 and CO_2,

$$CH_3OCH_2OCH_3 + H_2O = 2CH_3OH + CH_2O, \quad (1)$$

$$CH_3OH + H_2O = 3H_2 + CO_2, \quad (2)$$

$$CH_2O + H_2O = 2H_2 + CO_2. \quad (3)$$

The overall reaction can then be expressed as

$$CH_3OCH_2OCH_3 + 4H_2O = 8H_2 + 3CO_2. \quad (4)$$

Thus, the catalysts for the reforming of DMM must consist of a solid acid for the hydrolysis of DMM and a component for the reforming of methanol and formaldehyde. The latter is usually $CuZnO/Al_2O_3$ (CuZnAl), which has been studied extensively [5–8]. The acidic component must be chosen carefully; it should effectively catalyze the hydrolysis of DMM, but not affect the performance of $CuZnO/Al_2O_3$ for the reforming reactions.

Niobium oxides and niobium phosphates have strong surface acidity and are used as solid acid catalysts [21–24]. The acidity and reactivity of these systems have been studied by different techniques [25–33]. The preparation, characterization, and application of niobium-containing materials were reviewed by Nowak and Ziolek [21,22]. Tanabe summarized the catalytic applications of niobium compounds [23,24].

Niobium pentoxide (Nb_2O_5) is a white, air-stable, and water-insoluble solid that generally has an octahedrally coordinated NbO_6 distorted to different extent, depending on whether its polyhedra are corner-shared or edge-shared [34,35]. Hydrated niobium oxide ($Nb_2O_5{\cdot}nH_2O$) exhibits strong acidity according to the Hammett titration ($H_0 \leqslant -5.6$). Its acid strength is equivalent to about 70% sulfuric acid [36]. It has both Lewis and Brønsted acid sites [34]. The surface acid sites remain after outgassing at 673 K for 10 h, as determined by ammonia adsorption microcalorimetry [25]. It usually exhibits high activity for the acid-catalyzed reactions in which water molecules participate [36,37].

Niobium phosphate has a similar structure to Nb_2O_5 [21] but with higher acid strength ($H_0 \leqslant -8.2$). It has a distorted octahedra (NbO_6) connected by PO_4 tetrahedra via shared corners [22]. Both terminal POH and NbOH groups are present in bulk and impregnated niobium phosphate catalysts [22]. The POH are stronger Brønsted acids than NbOH in niobium phosphates [38]. The Lewis acid sites in niobium phosphates are coordinatively unsaturated Nb^{5+} cations [38].

Porous niobium oxides and niobium-containing materials can be synthesized by various methods [39–44]. Recently, porous niobium phosphates with high surface areas were prepared and used as solid acid catalysts by Mal and Fujiwara [45].

In this work, we prepared and characterized porous niobium phosphates and compared them with a niobium oxide and a commercial niobium phosphate (supplied by CBMM). The surface acidities of these samples were studied by adsorption microcalorimetry of ammonia, infrared spectroscopy (IR), and isopropanol probe reaction and were correlated with the activities for the hydrolysis of DMM. In addition, these samples were mixed with the traditional $CuZnO/Al_2O_3$ to form complex catalysts for the reforming of DMM to produce H_2.

2. Experimental

2.1. Catalyst preparation

Nb_2O_5 was prepared by calcining a commercial niobic acid ($Nb_2O_5{\cdot}nH_2O$, CBMM, Brazil) at 623 K for 4 h in flowing air. NbP1 is a commercial niobium phosphate provided by the CBMM in Brazil. NbP2 is a niobium phosphate prepared by the impregnation method [38]. In short, 6.35 g of niobic acid was added to 120 ml of aqueous solution of H_3PO_4 (1 M) and stirred for 48 h at room temperature. The slurry was filtered, dried at 373 K overnight, and then calcined at 673 K for 4 h. A high-surface area niobium phosphate (NbP3) was prepared as described previously [45]. Specifically, 2.73 g of $NbCl_5$ (Alfa Aesar, 99%) was partially hydrolyzed in 50 ml of H_2O, followed by the addition of 2.30 g of H_3PO_4 (Aldrich, 85% aqueous solution) to initiate a vigorous hydrolytic reaction. An additional 50 ml of H_2O was then added, and the reaction mixture was stirred for 30 min. The pH of the reaction mixture was adjusted to 2.60 by ammonia solution. After stirring, the slurry was filtered and washed with deionized water to obtain a chlorine-free gel. The gel was mixed with 10 ml of H_2O and 1.45 g of hexadecylamine (Aldrich, 90%) and stirred for 30 min. Then 0.92 g H_3PO_4 (85%) was added, and the pH of the mixture was adjusted to 3.88. After mixing was complete, the slurry was heated in a Teflon-lined stainless steel autoclave at 338 K under autogenous pressure for 2 days. The final product was filtered, washed with deionized water, dried at 373 K overnight, and calcined at 723 K in air for 40 h. $CuZnO/Al_2O_3$ is a commercial catalyst (CF105, a product of the Research Institute of Nanjing Chemical Industry Group, China) with a molar ratio of 63% Cu, 21% Zn, and 16% Al.

2.2. Catalyst characterization

The X-ray diffraction (XRD) measurements were done using a Bruker D5005 diffractometer scanning from 3° to 80° (2θ) at a rate of 0.02 degree s^{-1} and from 1° to 10° (2θ) at a rate of 0.002 degree s^{-1} using a Cu$K\alpha$ radiation ($\lambda = 0.15418$ nm) source. The applied voltage and current were 50 kV and 35 mA, respectively. Elemental analysis was performed by ICP atomic emission spectroscopy (Spectroflame-ICP D, Spectro). The surface area and pore size were measured by nitrogen adsorption at 77 K after heat pretreatment under vacuum at 623 K for 4 h. Transmission electron microscopy (TEM) was done using a JEM 2010 operating at 200 kV in bright- and dark-field modes. The X-ray photoelectron spectra (XPS) were measured on a SSI 301 instrument equipped with a hemispherical electron analyzer and an Al anode (Al$K\alpha = 1486.6$ eV) powered at 100 W. The residual pressure in the spectrometer chamber during data acquisition was 5×10^{-8} Pa.

The microcalorimetric studies of ammonia adsorption were performed at 423 K in a heat flow calorimeter (Setaram C80) linked to a conventional volumetric apparatus equipped with

a Barocel capacitance manometer for pressure measurements. Ammonia used for measurements (purity >99.9%) was purified by successive freeze–pump–thaw cycles. About 100 mg of sample was pretreated in a quartz cell under evacuation overnight at 623 K. The differential heat of adsorption was measured as a function of coverage by repeatedly introducing small doses of ammonia gas onto the catalyst until an equilibrium pressure of about 66 Pa was reached [46]. The sample was then outgassed for 30 min at the same temperature, and a second adsorption was performed at 423 K until an equilibrium pressure of about 27 Pa was attained, to calculate the irreversibly chemisorbed amount of ammonia at this pressure, which gives an estimation of number of strong acid sites.

Temperature-programmed ammonia desorption was performed on a Setaram TG-DSC 111 device coupled with a mass spectrometer (Thermostar, Pfeifer) as a detector. A capillary-coupling system was used. The TPD experiments were carried out in a flow with helium as the carrier gas (10 ml min^{-1}). For each experiment, about 30 mg of a sample with ammonia absorbed in previous microcalorimetric experiments was used. Initially, the samples were purged with He at 373 K for 30 min to remove most of absorbed water and heated at 5 K min^{-1} in He up to 873 K. During this temperature increase, the mass spectrometer was set at $m/e = 15$, to avoid the interference of water fragmentation masses.

The NH_3 adsorption IR spectra were recorded with a Bruker Vector 22 FTIR spectrophotometer (DTGS detector) with a range of 4000–400, a resolution of 2 cm^{-1}, and 50 acquisition scans. The self-supporting wafer (10–30 mg, 18 mm diameter) was activated in situ in the IR cell at 673 K in flowing O_2 for 12 h, evacuated at the same temperature for 2 h, and then exposed to NH_3 (purity >99.9%) at room temperature for 5 min. Desorption was carried out by evacuation for 30 min at room temperature, 323, 373, 473, 523, 573, and 673 K. A spectrum was recorded at room temperature after desorption at each temperature.

2.3. Catalytic reaction

An isopropanol probe reaction carried out in a fixed-bed glass tube reactor was used to characterize the surface acidity. About 100 mg of sample was loaded for the reaction. Isopropanol was introduced to the catalysts by bubbling N_2 (99.999%) or air through a glass saturator filled with isopropanol maintained at 295 K. Isopropanol and reaction products were analyzed by an on-line gas chromatograph, using a PEG 20M packed column connected to a flame ionization detector (FID). Each catalyst was pretreated by heating in N_2 or air at 673 K for 1 h and then cooled in the same flow to the reaction temperature.

The hydrolysis of DMM was performed in a glass fixed-bed microreactor with an inner diameter of 6 mm. The DMM and H_2O were introduced to the reaction zone by bubbling N_2 (99.999%) through a glass saturator filled with DMM (Aldrich, 99%) maintained at 273 K and a glass saturator filled with H_2O maintained at 333 K. In each test, 50 mg of catalyst was loaded, and a gas hourly space velocity (GHSV) of 90,000 ml g^{-1} h^{-1} was used. The feed composition was maintained at N_2:H_2O:DMM = 24:5:1 (v/v). The tail gas out of the reactor was analyzed by an on-line gas chromatograph equipped with an FID and a Porapak N column for the separation of methanol, DMM, and other organic compounds. The gas lines were kept at 373 K to prevent condensation of the reactant and products. The reaction was carried out at atmospheric pressure.

The steam reforming of methanol (or DMM) was carried out in a same way as the hydrolysis of DMM. An acidic component was mixed with $CuZnO/Al_2O_3$ in a weight ratio of 1/7. About 500 mg of catalyst was loaded, and the GHSV was 10,000 ml g^{-1} h^{-1} for methanol and 4550 ml g^{-1} h^{-1} for DMM. The feed composition was maintained at N_2:H_2O:methanol = 8.8:1.25:1 or N_2:H_2O:DMM = 24:5:1 (v/v). The products were analyzed by an on-line gas chromatograph equipped with an FID and a thermal conductivity detector (TCD). The FID was connected to a Porapak N column for the separation of methanol, DMM, and other organic compounds, whereas the TCD was connected to a TDX-01 column for the analysis of methane, CO_x, and N_2. The amount of H_2 produced was usually calculated according to the conversion of DMM and the composition of other products and was checked using another gas chromatograph.

3. Results and discussion

3.1. Structural characterizations

The XRD results shown in Fig. 1 indicated that the Nb_2O_5 and niobium phosphate samples studied in this work were amorphous. They exhibited mainly two broad 2θ peaks at around 25° and 52°. The peaks were shifted to lower angles for the sample NbP3, implying some difference in bonding in this high-surface area sample.

Results of bulk and surface elemental analysis, as well as the surface area and porosity data for the samples, are given in Table 1. The NbP3 prepared using a template had a significantly greater surface area (394 m^2 g^{-1}) than the other samples. In addition, chemical analysis showed that this sample had a much higher P content (12.4 wt%), which is close to the Nb/P atomic ratio of 1/1, than the other niobium phosphate samples. XPS results indicated that P might be slightly enriched on the surface of these niobium phosphate samples.

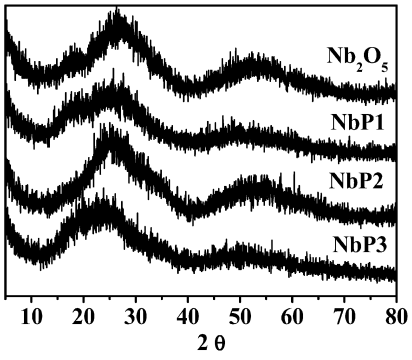

Fig. 1. X-ray diffraction (XRD) patterns of Nb_2O_5 and niobium phosphate catalysts.

Table 1
Chemical analysis, X-ray photoelectron spectroscopic data, BET surface area, and average pore radius of the samples

Sample	C.A. (wt%)		XPS (AT%)		BET ($m^2\ g^{-1}$)	Average pore radius (nm)
	Nb	P	Nb	P		
Nb_2O_5	69.2	–	–	–	110	Not determined
NbP1	46.6	5.0	13.4	8.9	142	3.0
NbP2	46.7	4.0	18.7	5.6	81	Not determined
NbP3	42.6	12.4	12.1	12.7	394	<1.5

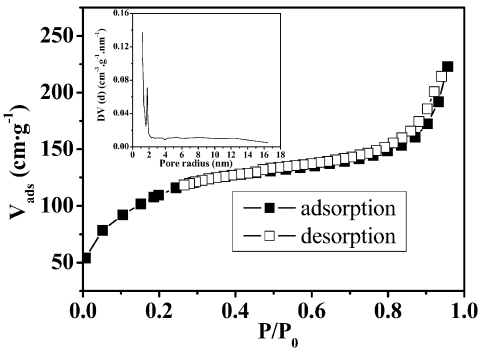

Fig. 2. N_2 adsorption–desorption isotherms of NbP3. (Inset: Pore radius distribution curve from the desorption branch of the isotherm.)

The N_2 adsorption–desorption isotherms and pore size distribution for NbP3 are depicted in Fig. 2. The adsorption–desorption isotherms are similar to type II and show no significant hysteresis loop, explaining the "supermicroporous" nature of the sample as suggested by Blanchard et al. [47]. The results agree well with those reported by Mal and Fujiwara [45]. The pore radius thus measured for NbP3 was <1.5 nm, which is lower than that of NbP1 (3 nm), a niobium phosphate provided by CBMM. The small-angle XRD showed the two diffraction peaks at $2\theta = 1.9$ and 4.2 for the NbP3 before calcination, corresponding to (100) and (110) reflections [45] and indicating the ordered structure of NbP3.

The TEM images of Nb_2O_5 and NbP3 are shown in Fig. 3. Both samples exhibit pore structures with diameters of 1–5 nm.

Temperature-programmed reduction experiments revealed no significant hydrogen consumption peaks for the Nb_2O_5 and niobium phosphates up to 1100 K, indicating that reduction of these samples was difficult [22].

The skeletal IR spectra are reported in Fig. 4. All of the samples exhibited a band around 1628 cm^{-1}, due to the scissoring mode of adsorbed molecular water. A sharp band at around 1385 cm^{-1} for NbP1, probably due to the O–C–O symmetric vibration of impurities of potassium carbonate in NbP1 (a commercial product), can be seen. This peak was also observed for the other three samples, although its intensity was weak. Chemical analysis showed that the niobic acid from CBMM contained a small amount of K (0.1%). Thus, the samples prepared using the niobic acid may contain K_2CO_3 formed during the preparation stage. In addition, all of the samples exhibited a broad band at around 600 cm^{-1}, probably due to the Nb–O–Nb stretching mode related to the slightly disordered octahedral NbO_6. A broad band around 1000 cm^{-1} was observed for Nb_2O_5 and NbP2, which could be assigned to the stretching

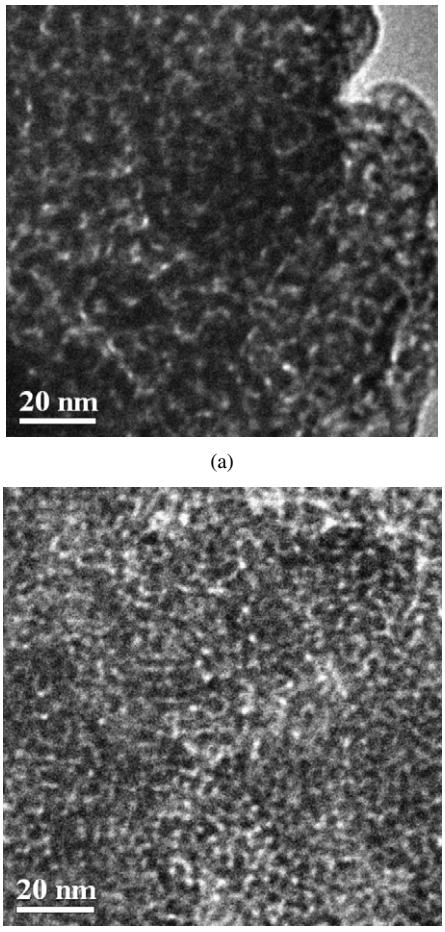

(a)

(b)

Fig. 3. Transmission electron microscopy (TEM) images of (a) Nb_2O_5 and (b) NbP3.

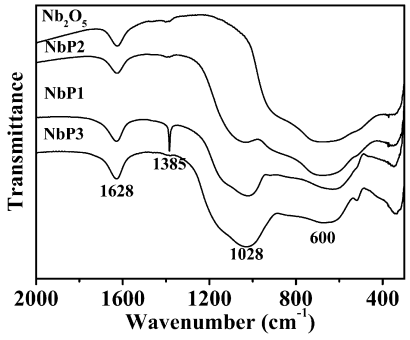

Fig. 4. FTIR skeletal spectra (KBr pressed disks with 2 mg sample in 198 mg KBr) of Nb_2O_5 and NbP catalysts.

mode of the short Nb=O bond in a highly disordered octahedral NbO_6. The different extent of NbO_6 disordering may suggest the stability of NbO_6 on the addition of P [21,22]. Furthermore, the addition of P to Nb_2O_5 also resulted in an additional broad band located at around 1028 cm^{-1}, possibly due to the O=P=O asymmetric stretching mode of phosphate or polyphosphate species. The intensity of this band increased with increasing P content in NbP. These results agree well with those reported by Armaroli et al. [38].

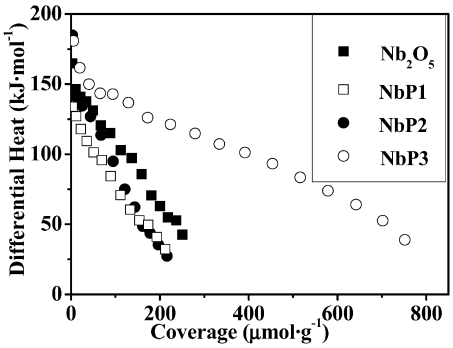

Fig. 5. Differential heat versus coverage (in μmol g^{-1}) for ammonia adsorption at 423 K over Nb_2O_5 and niobium phosphate catalysts.

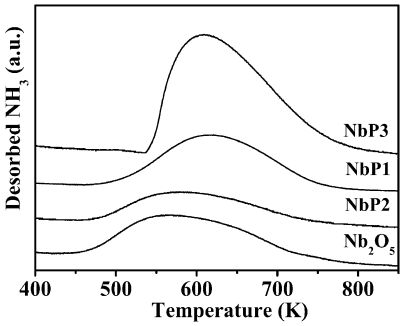

Fig. 6. Temperature-programmed desorption (TPD) profiles of adsorbed NH_3 on Nb_2O_5 and niobium phosphate catalysts.

3.2. Surface acidity

Surface acidity, in terms of number of acid sites and site strengths, was titrated by adsorption microcalorimetry of ammonia; the results are presented in Fig. 5. The initial heat for ammonia adsorption on Nb_2O_5 was found to be about 165 kJ mol^{-1}, which is higher than that of acidic solids such as γ-Al_2O_3. In fact, Nb_2O_5 is considered a strong acid according to Hammett titration [36]. The two niobium phosphate samples, NbP1 and NbP2, behaved similarly to Nb_2O_5 in terms of the heat versus coverage curves for ammonia adsorption, indicating that the addition of P to Nb_2O_5 did not seem to enhance surface acidity. However, the saturation coverage of ammonia on NbP3 was found to be about 750 μmol g^{-1}, much higher than that for the other samples in this work. This is apparently due to the much higher surface area of NbP3 as compared with the other samples. In fact, when the surface coverage was expressed in terms of the amount of ammonia adsorbed on a unit surface area, the coverage on NbP3 was lower than that on other samples.

Fig. 6 shows the NH_3-TPD results for the Nb_2O_5 and niobium phosphate samples. All of the samples exhibited a desorption peak so broad as to reveal the heterogeneous strength distribution of the acid sites in these samples. It is usually not accurate to rank the acid strengths by simply comparing the desorption maxima because of the complex diffusion effect, especially for the porous materials. However, the temperatures of the peak maxima were higher for the niobium phosphate samples than for Nb_2O_5, implying the stronger acidity of niobium phosphate compared with Nb_2O_5. In addition, the areas of desorption peaks reflected the relative populations of acid sites. It is clearly shown that the NbP3 had many more acid sites than the other samples, agreeing well with the microcalorimetric adsorption results.

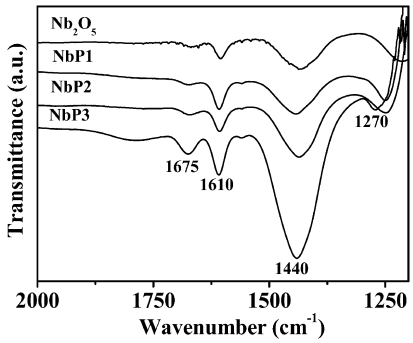

Fig. 7. FTIR spectra for NH_3 adsorption and desorption at room temperature on Nb_2O_5 and niobium phosphate catalysts.

Table 2
Results of isopropanol probe reaction in N_2 at 413 K

Sample	Conversion (%)	Selectivity (%)		
		PPE	DIPE	ACE
Nb_2O_5	0.3	81.0	19.0	0
NbP1	1.0	74.5	25.5	0
NbP2	2.0	74.8	25.2	0
NbP3	15.2	78.3	21.7	0

Note. PPE, DIPE, and ACE denote propylene, diisopropyl ether, and acetone, respectively.

Fig. 7 shows the FTIR spectra of the samples for ammonia adsorption. Both Brønsted and Lewis acid sites were present on the samples. The bands at around 1675 and 1440 cm^{-1} were due to the deformation vibration of NH_4^+ formed by the interaction of NH_3 with Brønsted acid sites, whereas the bands at 1610 and 1270 cm^{-1} originated from the asymmetric and symmetric deformation vibrations, respectively, for NH_3 coordinated to Nb^{5+}. IR spectra from adsorbed pyridine [48] and acetonitrile [38] also revealed the presence of both Brønsted and Lewis acidity on niobium phosphates. It should be mentioned that the NbP3 sample seemed to exhibit more Brønsted acid sites than the other samples according to the relative intensities of the peak at around 1440 cm^{-1}. On evacuation at 473 K, all of the IR peaks for adsorbed ammonia disappeared for the Nb_2O_5, NbP1, and NbP2 samples, whereas these peaks remained for the NbP3 sample (data not shown). These results indicate that the NbP3 sample exhibited the strongest surface acidity of all the samples studied in this work.

3.3. Isopropanol probe reaction

The results of isopropanol (IPA) probe reaction over the samples in flowing N_2 are presented in Table 2 and Fig. 8. It is well known that IPA undergoes dehydration reactions to produce propylene (PPE) and diisopropyl ether (DIPE) on acid sites, and undergoes a dehydrogenation reaction to acetone (ACE) on base sites in inert atmosphere [49,50]. Thus, the con-

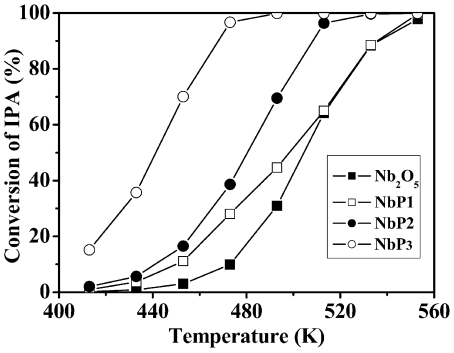

Fig. 8. Conversion of isopropanol (IPA) in N_2 at different temperatures over Nb_2O_5 and niobium phosphate catalysts.

version of IPA and selectivity to PPE, DIPE, and ACE in N_2 can be used to probe the strengths of surface acidity and basicity. In addition, IPA can also be oxidatively dehydrogenated to ACE in an oxidation atmosphere, which can be used to probe the surface redox properties.

Results in Table 2 show that the Nb_2O_5 and niobium phosphates exhibited only surface acidity, because only the products PPE and DIPE were formed. The conversion of IPA was significantly higher on the niobium phosphate samples than on Nb_2O_5, indicating that niobium phosphates are more acidic than Nb_2O_5. In addition, NbP3 exhibited much higher IPA conversion than the other niobium phosphates. Fig. 8 compares the conversion of IPA at different temperatures over the Nb_2O_5 and niobium phosphates. The results clearly show that NbP3 was much more active than the other samples over the whole range of reaction temperatures. Below 500 K, NbP1 and NbP2 were also more active than Nb_2O_5. Further data showed that IPA probe reaction over Nb_2O_5 and niobium phosphates in both N_2 and air did not produce any ACE, indicating that these samples were neither basic nor oxidative under the reaction conditions. The conversions of IPA and selectivity were similar for the reaction performed in N_2 and air. These results are not completely consistent with those of microcalorimetric adsorption of ammonia presented above; the inconsistency may be due to the different treatments in the experiments for microcalorimetric adsorption and the probe reaction. The evacuation treatment for the microcalorimetric adsorption may have removed more hydroxyl groups on the surface of the samples, decreasing the surface acidity. On the other hand, the IPA dehydration reaction produced water and hydrolyzed the surface of the samples, possibly enhancing the surface acidity of the samples.

3.4. Hydrolysis of DMM

DMM is hydrolyzed to methanol (MeOH) and formaldehyde (FA) according to Eq. (1). Table 3 gives the results for the hydrolysis of DMM over the Nb_2O_5 and niobium phosphate catalysts. MeOH and FA were the main products, with selectivity >96%. Other products were DME and methyl formate (MF), with total selectivity <4%. The conversion of DMM increased with increasing temperature for all of the samples. At lower temperatures, the conversion of DMM was higher over the catalysts with higher surface acidity as probed by the IPA reaction. At temperatures above 493 K, the conversion of DMM approached 100% over all of the samples. Our previous studies revealed that at 493 K, DMM was converted mainly to MeOH and FA, with low conversion (<10%) on γ-Al_2O_3, whereas >75% of DMM was converted to DME over H-ZSM-5 even though the conversion was high (99%) [17]. Thus, the Nb_2O_5 and niobium phosphate catalysts seemed to be active and suitable for the hydrolysis of DMM and may be used as acidic components with the traditional CuZnAl catalyst for the reforming of DMM to produce H_2. DMM itself did not hydrolyze without a catalyst at temperatures as high as 533 K.

Table 3
Conversion and selectivity for the hydrolysis of DMM over the Nb_2O_5 and NbP catalysts

Sample	Temperature (K)	Conversion (%)	Selectivity (%)		
			DME	MF	MeOH and FA
Nb_2O_5	413	49	0.8	3	97
	433	63	0.6	4	96
	453	77	0.4	3	97
	473	86	0.3	3	97
	493	94	0.5	3	97
	513	98	0.4	2	98
	533	100	0.4	2	98
NbP1	413	70	0.7	1	98
	433	82	0.7	3	96
	453	87	0.5	2	97
	473	93	0.6	2	97
	493	97	0.6	3	97
	513	99	0.5	3	97
	533	100	0.5	1	98
NbP2	413	72	1	0.0	99
	433	80	0.9	0.2	99
	453	87	1	0.2	99
	473	92	0.5	0.2	99
	493	98	1	0.2	99
	513	99	0.8	0.2	99
	533	100	0.6	0.2	99
NbP3	413	78	1	0.0	99
	433	87	0.6	0.4	99
	453	93	0.8	1	98
	473	95	0.8	0.4	99
	493	99	1	0.4	99
	513	99	1	0.2	99
	533	100	0.9	0.1	99

Note. DME, MF, MeOH, and FA denote dimethyl ether, methyl formate, methanol, and formaldehyde, respectively. Reaction conditions: $N_2/H_2O/DMM = 24/5/1$ (v/v), GHSV = 90,000 ml g^{-1} h^{-1}.

3.5. Reforming of methanol

Traditional CuZnAl catalyst is usually used for the reforming of methanol to produce H_2 [5–8]. The catalyst has been characterized in detail and used for the reforming of methanol by Murcia-Mascaros et al. [51] and Turco et al. [52]. In the present work, we examined the effect of adding Nb_2O_5 and NbP3 on the reforming of methanol over CuZnAl. The results, given in Fig. 9, clearly show that the addition of Nb_2O_5 or NbP3 did not affect the conversion of methanol on CuZnAl at 453–

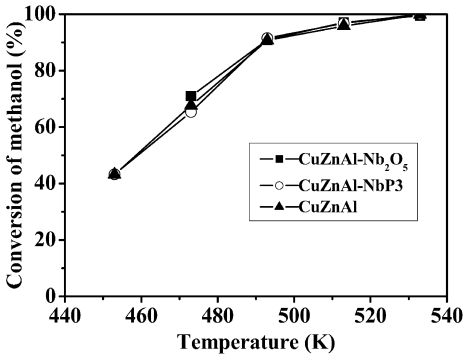

Fig. 9. Reforming of methanol over CuZnAl–Nb_2O_5 and CuZnAl–NbP catalysts.

533 K. In addition, no DME or other organic compounds were observed for the reforming of methanol on these catalysts. The only products detected were CO_x and H_2. Thus, both Nb_2O_5 and NbP seem to be suitable hydrolysis components for the reforming of DMM.

3.6. Reforming of DMM

We mixed an industrial CuZnAl catalyst with our Nb_2O_5 and NbP3 to form the complex catalysts for the reforming of DMM. The weight ratio of CuZnAl to acid component was 7/1, and a complex catalyst contained only 12.5% of the acidic component. This is because the hydrolysis of DMM on the acidic components was rapid, as discussed above. A GHSV of 4550 ml g^{-1} h^{-1} was used for the complex catalysts, corresponding to the GHSV of 36,400 ml g^{-1} h^{-1} on the acid component, which was lower than that for the hydrolysis of DMM (90,000 ml g^{-1} h^{-1}) used above. Thus, the rate of DMM reforming on the complex catalysts should be limited mainly by the methanol reforming on the CuZnAl component.

Table 4 shows that the CuZnAl catalyst exhibited low conversion for the reforming of DMM and produced a substantial amount of DME. Addition of either a niobium oxide or NbP3 component greatly enhanced the conversion of DMM and inhibited the formation of DME. For example, almost no DMM conversion was observed on the CuZnAl at 453 K, whereas the DMM conversion was 94% at this temperature with the addition of Nb_2O_5. The conversion of DMM reached 100% on the CuZnAl–NbP3 at 453 K. These results clearly demonstrate that the acidic component is essential for the reforming of DMM. Below 493 K, methanol was detected in the products for the reforming of DMM on CuZnAl–Nb_2O_5 or CuZnAl–NbP3, revealing that the rate of DMM hydrolysis was faster than that of methanol reforming. Thus, the reforming of methanol appears to be the rate-determining step for the reforming of DMM below 493 K. Above 493 K, the rate of reforming of methanol on CuZnAl was sufficiently fast so that no methanol was detected. The rate of hydrogen production was also significantly improved by the addition of an acidic niobium component. The highest rate of H_2 production obtained in this work for the reforming of DMM was 1185 ml g^{-1} h^{-1} at 493 K, which was lower than 2438 ml g^{-1} h^{-1} for the reforming of methanol at the same temperature. This does not mean that the rate of H_2 production from the reforming of DMM is always lower than that from the reforming of methanol. The rate of H_2 production depends on the activity of catalysts and the space velocity of feed gas. A thorough comparison between the reforming of DMM and that of methanol for the production of H_2 requires data for the complete conversion of DMM and methanol at the maximum space velocities. The rate of H_2 production from the reforming of DMM over the CuZnAl–H-CNF (where H-CNF denotes acidic carbon nanofiber) was found to be about 80% of that from the reforming of methanol on the CuZnAl [17].

3.7. CO concentration and the water–gas shift reaction

CO concentration is a critical issue for fuel cell applications, because one of the most promising types of fuel cells, the

Table 4
Conversion and selectivity for the steam reforming of DMM over the CuZnAl and hybrid catalysts (CuZnAl/acid component = 7/1 wt)

Sample	Temperature (K)	Conversion (%)	Selectivity (%)					R_{H_2} (ml g^{-1} h^{-1})
			CH_4	DME	MeOH	CO	CO_2	
CuZnAl–Nb_2O_5	453	94	0	0	61	0	39	620
	473	100	0	0	9	1	90	1116
	493	100	0	0	0	3	97	1174
	513	100	0	0	0	5	95	1156
	533	100	0	0	0	6	94	1141
CuZnAl–NbP3	453	100	0	0.1	45	0	55	803
	473	100	0	0.1	3	2	95	1163
	493	100	0	0.1	0	2	98	1185
	513	100	0	0.1	0	4	96	1159
	533	100	0	0.1	0	6	94	1146
CuZnAl	453	1.5	1	19	8	0	72	14
	473	4.7	1	16	7	0	76	47
	493	11	1	21	6	0	72	106
	513	31	0.4	13	1	0.9	84	330
	533	47	1	22	1	2	75	458

Note. DME, MeOH, and R_{H_2} denote dimethyl ether, methanol, and rate of hydrogen production, respectively. Reforming conditions: $N_2/H_2O/DMM = 24/5/1$ (v/v), GHSV = 4550 ml g^{-1} h^{-1}.

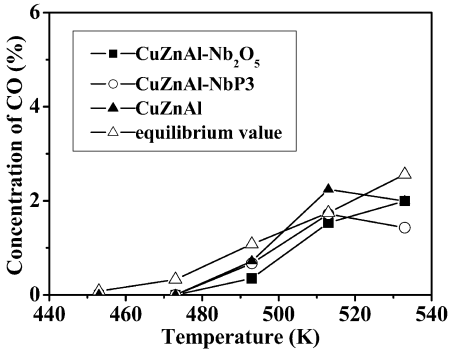

Fig. 10. Concentration of CO in products over CuZnAl–Nb_2O_5 and CuZnAl–NbP3 catalysts for the reforming of methanol.

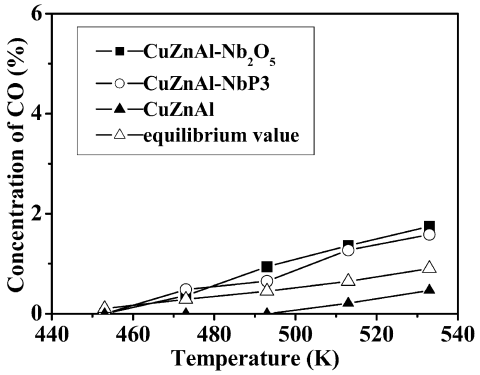

Fig. 11. Concentration of CO in products over CuZnAl–Nb_2O_5 and CuZnAl–NbP3 catalysts for the reforming of DMM.

proton-exchange-membrane fuel cell (PEMFC), is extremely susceptible to poisoning by CO in the anode feed gas. CO concentrations <10 ppm are desirable in a fuel for a PEMFC. Figs. 10 and 11 show that the selectivity to CO increased with increasing of temperature for the reforming of both methanol and DMM, possibly due to the reversed water gas shift reaction (RWGSR: $CO_2 + H_2 = CO + H_2O$) shift to the right with increasing temperature. In fact, the concentration of CO in the tail gas from the reforming of methanol or DMM is close to the equilibrium value, and the maximum CO concentration is <2%. It seemed that the addition of niobium component did not affect the equilibrium of the RWGSR over CuZnAl. The concentration of CO in the tail gas is known to depend on the concentration of H_2O in the feed gas for the reforming of methanol. When the concentration of H_2O is insufficient in the feed gas, methanol directly decomposes to CO and H_2 on CuZnAl, and the rate of such decomposition is much slower than that of the reforming of methanol [53]. On the other hand, excessive H_2O would entail excessive energy costs. This situation also holds for the reforming of DMM, because it involves the hydrolysis of DMM and the reforming of methanol. The ratios of H_2O/methanol and H_2O/DMM applied in this work were 2 and 5, respectively, slightly higher than the respective stoichiometric ratios (1 and 4), to minimize the CO concentrations without entailing an excessive energy cost.

4. Conclusion

Niobium phosphates were prepared by different methods in which porous NbOPO4 with high surface area (394 $m^2\,g^{-1}$) was obtained using hexadecylamine as a template. The Nb_2O_5 and niobium phosphate samples studied in this work had similar amorphous structures. The niobium phosphates were found to be more acidic than Nb_2O_5, especially that with a high surface area. Both Brønsted and Lewis acid sites were present on the surface of Nb_2O_5 and niobium phosphates, with niobium phosphates having more Brønsted sites than Nb_2O_5. The high-surface area niobium phosphate exhibited numerous surface acid sites (~750 μmol g^{-1}) and was active in catalyzing the dehydration of isopropanol and the hydrolysis of DMM. The complex catalysts resulting from combining Nb_2O_5 or niobium phosphate with an industrial $CuZnO/Al_2O_3$ were effective for the reforming of DMM to produce H_2 at above 493 K. DMM could be completely reformed into CO_x and H_2 over the complex catalysts at 493 K. Because DMM is more environmentally benign than methanol, our findings indicate that it is possible to reform DMM directly using a proper acidic component with the traditional $CuZnO/Al_2O_3$ catalyst.

Acknowledgments

The authors acknowledge financial support from CNRS-France, the French Ministry of Education, the French–Chinese joint program PRA E 03-01, and the Ministry of Science and Technology of China (Grants 2004DFB02900 and 2005 CB221400).

References

[1] P.G. Gray, M.I. Petch, Platinum Metals Rev. 44 (2000) 108.
[2] S. Golunski, Platinum Metals Rev. 42 (1998) 2.
[3] N. Edwards, S.R. Ellis, J.C. Frost, S.E. Golunski, A.N.J. van Keulen, N.G. Lindewald, J.G. Reinkingh, J. Power Sources 71 (1998) 123.
[4] A.D. Qi, S.D. Wang, G.Z. Fu, C.J. Ni, D.Y. Wu, Appl. Catal. A 281 (2005) 233.
[5] J.C. Amphlett, M.J. Evans, R.A. Jones, R.F. Mann, R.D. Weir, Can. J. Chem. Eng. 59 (1981) 720.
[6] B. Emonts, J.B. Hansen, S.L. Jorgensen, B. Hohlein, R. Peters, J. Power Sources 71 (1998) 288.
[7] T. Takeguchi, Y. Kani, M. Inoue, K. Eguchi, Catal. Lett. 83 (2002) 49.
[8] J.-P. Shen, C.S. Song, Catal. Today 77 (2002) 89.
[9] K. Takeishi, H. Suzuki, Appl. Catal. A 260 (2004) 111.
[10] V.V. Galvita, G.L. Semin, V.D. Belyaev, T.M. Yurieva, V.A. Sobyanin, Appl. Catal. A 216 (2001) 85.
[11] V.A. Sobyanin, S. Cavallaro, S. Freni, Energy Fuels 14 (2000) 1139.
[12] S.F. Yin, B.Q. Xu, X.P. Zhou, C.T. Au, Appl. Catal. A 277 (2004) 1.
[13] T.V. Choudhary, C. Sivadinarayana, D.W. Goodman, Catal. Lett. 72 (2001) 197.
[14] F. Vitse, M. Cooper, G.G. Botte, J. Power Sources 142 (2005) 18.
[15] C.S. Song, K.M. Reddy, Appl. Catal. A 176 (1999) 1.
[16] K. Klier, Adv. Catal. 31 (1982) 243.
[17] Y.C. Fu, Studies of Some Catalytic Reactions for the Synthesis and Conversion of Methanol-Derived Chemicals, Ph.D. thesis, Nanjing University, 2005.
[18] H.C. Liu, N. Bayat, E. Iglesia, Angew. Chem. Int. Ed. 42 (2003) 5072.
[19] Y.Z. Yuan, H.C. Liu, H. Imoto, T. Shido, Y. Iwasawa, J. Catal. 195 (2000) 51.
[20] Y.Z. Yuan, T. Shido, Y. Iwasawa, Chem. Commun. 15 (2000) 1421.

[21] I. Nowak, M. Ziolek, Chem. Rev. 99 (1999) 3603.
[22] M. Ziolek, Catal. Today 78 (2003) 47.
[23] K. Tanabe, S. Okazaki, Appl. Catal. A 133 (1995) 191.
[24] K. Tanabe, Catal. Today 78 (2003) 65.
[25] P. Carniti, A. Gervasini, S. Biella, A. Auroux, Chem. Mater. 17 (2005) 6128.
[26] K. Asakura, Y. Iwasawa, Chem. Lett. (1986) 859.
[27] J.M. Jehng, A.M. Turek, I.E. Wachs, Appl. Catal. A 83 (1992) 179.
[28] A. Florentino, P. Cartraud, P. Magnoux, M. Guisnet, Appl. Catal. A 89 (1992) 143.
[29] T. Ushikubo, T. Iizuka, H. Hattori, K. Tanabe, Catal. Today 16 (1993) 291.
[30] T. Tanaka, H. Nojima, H. Yoshida, H. Nakagawa, T. Funabiki, S. Yoshida, Catal. Today 16 (1993) 297.
[31] J.C. Vedrine, G. Coudurier, A. Ouqour, P.G.P. de Oliveira, J.C. Volta, Catal. Today 28 (1996) 3.
[32] P. Batamack, R. Vincent, J. Fraissard, Catal. Lett. 36 (1996) 81.
[33] C.L.T. da Silva, V.L.L. Camorim, J.L. Zotin, M. Pereira, A.D. Faro, Catal. Today 57 (2000) 209.
[34] J.-M. Jehng, I.E. Wachs, Catal. Today 8 (1990) 37.
[35] J.-M. Jehng, I.E. Wachs, Chem. Mater. 3 (1991) 100.
[36] K. Tanabe, Mater. Chem. Phys. 17 (1987) 217.
[37] K. Tanabe, Catal. Today 8 (1990) 1.
[38] T. Armaroli, G. Busca, C. Carlini, M. Giuttari, A.M.R. Galletti, G. Sbrana, J. Mol. Catal. A 151 (2000) 233.
[39] D.M. Antonelli, J.Y. Ying, Angew. Chem. Int. Ed. Engl. 35 (1996) 426.
[40] M. Ziolek, I. Nowak, J.C. Lavalley, Catal. Lett. 45 (1997) 259.
[41] R. Abe, K. Shinohara, A. Tanaka, M. Hara, J.N. Kondo, K. Domen, J. Mater. Res. 13 (1998) 861.
[42] D.M. Antonelli, Micropor. Mesopor. Mater. 33 (1999) 209.
[43] B. Lee, D.L. Lu, J.N. Kondo, K. Domen, J. Am. Chem. Soc. 124 (2002) 11256.
[44] S. Murray, M. Trudeau, D.M. Antonelli, Adv. Mater. 12 (2000) 1339.
[45] N.K. Mal, M. Fujiwara, Chem. Commun. (2002) 2702.
[46] A. Auroux, Top. Catal. 4 (1997) 71.
[47] J. Blanchard, F. Schuth, P. Trens, M. Hudson, Micropor. Mesopor. Mater. 39 (2000) 163.
[48] S. Okazaki, N. Wada, Catal. Today 16 (1993) 349.
[49] A. Gervasini, J. Fenyvesi, A. Auroux, Catal. Lett. 43 (1997) 219.
[50] X.D. Gu, C. Hui, J.Y. Shen, Chin. J. Catal. 24 (2003) 885.
[51] S. Murcia-Mascaros, R.M. Navarro, L. Gomez-Sainero, U. Costantino, M. Nocchetti, J.L.G. Fierro, J. Catal. 198 (2001) 338.
[52] M. Turco, G. Bagnasco, U. Costantino, F. Marmottini, T. Montanari, G. Ramis, G. Busca, J. Catal. 228 (2004) 43.
[53] B.A. Peppley, J.C. Amphlett, L.M. Kearns, R.F. Mann, Appl. Catal. A 179 (1999) 21.